CONDENSED MATTER PHYSICS

Topological materials discovery by large-order symmetry indicators

Feng Tang[1,2], Hoi Chun Po[3,4], Ashvin Vishwanath[3], Xiangang Wan[1,2]*

Crystalline symmetries play an important role in the classification of band structures, and their richness leads to various topological crystalline phases. On the basis of our recently developed method for the efficient discovery of topological materials using symmetry indicators, we explore topological materials in five space groups (SGs), which are diagnosed by large-order symmetry indicators ($\mathbb{Z}_8$ and $\mathbb{Z}_{12}$) and support the coexistence of several kinds of gapless boundary states in a single compound. We predict many candidate materials; some representatives include Pt_3Ge (SG 140), graphite (SG 194), XPt_3 (SG 221, X = Sn, Pb), Au_4Ti (SG 87), and Ti_2Sn (SG 194). As by-products, we also find that $AgXF_3$ (SG 140, X = Rb, Cs) and AgAsX (SG 194, X = Sr, Ba) are good Dirac semimetals with clean Fermi surfaces. The proposed materials provide a good platform for studying the novel properties emerging from the interplay between different types of boundary states.

INTRODUCTION

Since the discovery of two-dimensional (2D) and 3D topological insulators (TIs), band topology in condensed matter materials has attracted broad interest owing to their rich scientific implications and potential for technological applications (*1*, *2*). Described by $\mathbb{Z}_2$ topological invariant(s), time-reversal ($\mathcal{T}$) invariant TIs are characterized by an insulating gap in the bulk and $\mathcal{T}$-protected gapless states on the boundary of the system (*1*, *2*). Inspired by the discovery of TIs, it was realized that symmetries play a key role in the classifications of topological phases. On the basis of the absence or presence of $\mathcal{T}$, particle hole, or chiral symmetry, insulators and superconductors have been classified under the so-called 10-fold way (*3*).

In addition to the aforementioned internal symmetries, the topological classification of band structures has also been extended to include crystalline symmetries (*4*–*6*). Because of the vast array of crystal symmetries [encapsulated by the 230 crystalline space groups (SGs)], a massive number of topological crystalline phases (TCPs) have been proposed, such as mirror Chern insulators (*7*), quantized electric multipole insulators (*8*), high-order TIs (*9*, *10*), hourglass fermions (*11*), nodal-chain metals (*12*), and (semi-)metals with unconventional quasiparticles arising from threefold (or higher) band degeneracies (*13*).

Despite the large number of theoretically proposed TCPs, the discovered topological compounds represent a very small fraction of the experimentally synthesized materials tabulated in structure databases (*14*). Such apparent scarcity of topological materials originates from the theoretical difficulty in exhaustively computing topological band invariants in first-principles calculations, which becomes increasingly time consuming because of the expanding set of identified invariants (*4*–*7*, *9*, *11*, *15*–*23*). Hence, the prediction of any realistic topological materials is typically taken as a big achievement (*1*, *2*, *6*, *7*, *11*–*13*, *24*–*26*).

Recent theoretical advancement has greatly reshaped the landscape of materials discovery. By exploiting the mismatch between the real- and momentum-space descriptions of band structure, novel forms of band topology in the 230 SGs for nonmagnetic compounds (*27*, *28*) and the 1651 magnetic SGs for magnetic materials have been proposed (*29*). A main advantage of the formalism of symmetry-based indicators of band topology (*27*) is its compatibility with first-principles calculation: In stark contrast to conventional target-oriented searches, our algorithm does not presuppose any specific phase of matter. Based on symmetry representations, which can be readily computed using standard protocols, one can quickly discern topological (semi-)metals, TIs, and topological crystalline insulators from the database (*30*). The high efficiency of our method has been demonstrated in (*30*), in which we discuss many topological materials discovered on the basis of their nontrivial index in space groups with $\mathbb{Z}_2$ or $\mathbb{Z}_4$ strong factor, X^s_{BS}, in the symmetry indicator (SI) group.

In this work, we focus on SGs with $X^s_{BS} = \mathbb{Z}_8$ or $\mathbb{Z}_{12}$. One particularly interesting aspect of the materials candidates we present in this work is the coexistence of topological surface states originating from bulk-boundary correspondence (*1*, *2*) dictated by various kinds of spatial symmetries (*27*, *31*, *32*). These SIs are realized in SGs with a high degree of coexisting symmetries, such as (roto-)inversion, mirror reflection, screw, and glide. There are in total 12 and 6 SGs with strong $\mathbb{Z}_8$ and $\mathbb{Z}_{12}$ SI factor groups, respectively (*27*). Focusing on five SGs with $\mathbb{Z}_8$ or $\mathbb{Z}_{12}$ strong SI group (SGs **87**, **140**, **221**, **191**, and **194**), we search for interesting TCPs in a single sweep of a structure database (*14*) using the method delineated in (*30*). We only consider spin orbit (SO)–coupled nonmagnetic materials with ≤ 30 atoms in their primitive unit cell. We find a large number of TCPs with reasonably clean Fermi surfaces. In the following, we present and discuss six representative topological crystalline insulators (TCIs) and list others in Tables 1 and 2. Four good Dirac semimetal candidates are discussed at the end.

REVIEW OF SYMMETRY INDICATORS

We begin by providing a brief review on topological materials discovery using SIs (*30*). In this paradigm, the topological properties of materials can be assessed by computing the representations of the filled energy bands at high-symmetry momenta, which is a standard protocol in band structure calculations. More concretely, the representation content is encoded in a collection of integers, $n^{\alpha}_{\mathbf{k}}$, which can be written as a formal vector: $\mathbf{n} = (\nu, n^1_{\mathbf{k}_1}, n^2_{\mathbf{k}_1}, \ldots)$, where ν is the total number of the filled energy bands, the subscript $\mathbf{k}_1$, $\mathbf{k}_2$, …, $\mathbf{k}_N$ denotes the high-symmetry point (HSP) in the Brillouin zone, the superscript

[1]National Laboratory of Solid State Microstructures and School of Physics, Nanjing University, Nanjing 210093, China. [2]Collaborative Innovation Center of Advanced Microstructures, Nanjing University, Nanjing, 210093, China. [3]Department of Physics, Harvard University, Cambridge, MA 02138, USA. [4]Department of Physics, Massachusetts Institute of Technology, Cambridge, MA 02139, USA.
*Corresponding author. Email: xgwan@nju.edu.cn

1, 2, …, α_i, … refers to the irreducible representation (irrep) of little group at $\mathbf{k}_i$ point ($\mathcal{G}_{\mathbf{k}_i}$), and $n_{\mathbf{k}_i}^{\alpha_i}$ means the number of times an α_i irrep of $\mathcal{G}_{\mathbf{k}_i}$ appears among the filled bands.

The set of vectors $\mathbf{n}$ forms an abelian group (*27*, *33*). Moreover, for every $\mathcal{SG}$, there exists d_{AI} atomic insulator (AI) basis vectors ($\mathbf{a}_i$, $i = 1, 2, \ldots, d_{\mathrm{AI}}$) containing information of the group structure for the SI, denoted by X_{BS} in (*27*), according to the possible common factor C_i for $\mathbf{a}_i$ (*27*). One can always expand any vector $\mathbf{n}$ with respect to the AI basis vectors $\mathbf{a}_i$: $\mathbf{n}=\sum_{i=1}^{d_{\mathrm{AI}}} q_i\mathbf{a}_i$. The expansion coefficients of $\mathbf{n}$ on the AI basis can be classified into three cases (*30*). Case 1: The expansion coefficients q_i's are all integers; such materials might be adiabatically connected to a trivial AI, so we do not consider materials in this case. Case 2: The expansion coefficients q_i are not all integers, but all q_iC_i are integers; such materials are necessarily topological, and the results of (q_iC_i mod C_i) give the nonvanishing SI (*30*). Case 3: The q_iC_i are not all integers; such systems are (semi-)metallic. Specifically, if $n_{\mathbf{k}_i}^{\alpha}$ is noninteger, then there is band crossing happening at $\mathbf{k}_i$ point; on the other hand, if all the $n_{\mathbf{k}}^{\alpha}$ are integers, then there must be band crossing in the high-symmetry line or plane (*30*).

$\mathbb{Z}_8$ NONTRIVIAL TCI: Pt_3Ge

We now describe the promising TCP materials candidates we discovered. We first perform our materials search in the nonsymmorphic $\mathcal{SG}$**140** ($I4/mcm$), which has seven AI basis vectors: $\mathbf{a}_i^{\mathcal{SG}\mathbf{140}}$, $i = 1, 2, \ldots, 7$ (all the AI bases of the $\mathcal{SG}$s in this work are explicitly given in the Supplementary Materials). Only two AI basis vectors (we label them as $\mathbf{a}_6^{\mathcal{SG}\mathbf{140}}$ and $\mathbf{a}_7^{\mathcal{SG}\mathbf{140}}$) have nontrivial common factors: 2 and 8, respectively. Correspondingly, the SI group of $\mathcal{SG}$**140** is $X_{\mathrm{BS}}^{\mathcal{SG}\mathbf{140}} = \mathbb{Z}_2 \times \mathbb{Z}_8$. We list the relatively good materials belonging to case 2 in Table 1. In the following, we take Pt_3Ge as the example to analyze the detailed topological properties.

Pt_3Ge (ICSD[14] 077962) crystallizes in the body-centered tetragonal structure, where Ge occupies the 4*b* Wyckoff position, and Pt occupies two sets of inequivalent sites in the 4*a* and 8*h* Wyckoff positions. There are in total 68 valence electrons in the primitive unit cell. On the basis of ab initio calculation, we calculate the irrep multiplicities $n_{\mathbf{k}}^{\alpha}$ for all the HSPs and all the corresponding irreps α for the 68 valence bands. We then expand this calculated vector $\mathbf{n}$ on the seven AI basis vectors $\mathbf{n} = \sum_{i=1}^{7} q_i\mathbf{a}_i^{\mathcal{SG}\mathbf{140}}$ and obtain $q = \left(8, 0, 0, 1, 2, 1, -\frac{1}{2}\right)$. Thus, this material belongs to case 2 and is a TCI, with SI being (0,4). As seen from the electronic band plot in Fig. 1A, this material has large direct gaps through the k path.

While from SI alone we can ascertain that Pt_3Ge is a T(C)I, to resolve the concrete form of band topology it displays, we have to evaluate additional topological indices. First, we note that from the Fu-Kane parity criterion (*15*), one sees that the material cannot be a strong or a weak TI, and Pt_3Ge must be a TCI. As discussed in (*31*) and (*32*), the band topology of a TCI can be understood in terms of a collection of invariants associated to each of the elements of the space group. When the invariant of an element is nontrivial, one finds protected surface states on suitable surface terminations. For instance, if a glide invariant is nontrivial, one finds the hourglass surface states on surfaces respecting the glide symmetry (*11*). For symmetries like inversion and screws, which cannot leave any point invariant on the surface, their nontrivial invariants manifest as hinge states at suitable surface termination.

Table 1. Topological crystalline (TC) insulating materials for $\mathcal{SG}$s87, 140, and 221. These $\mathcal{SG}$s all own the same strong SI factor group, $\mathbb{Z}_8$, but with different other weak SI factor groups. The numbers in the parenthesis following the name of material are the nonvanishing SI in the corresponding X_{BS}. The SI is obtained by q_iC_i mod C_i, where $\mathbf{a}_i$ has a common factor larger than 1, which corresponds to the subscript of the factor groups of X_{BS}. The blue color denotes the materials carefully discussed in this work.

$\mathcal{SG}$	X_{BS}	Material (SI)
87	$\mathbb{Z}_2 \times \mathbb{Z}_8$	Au_4Ti (10), Hf_5Te_4 (11)
140	$\mathbb{Z}_2 \times \mathbb{Z}_8$	Pt_3Ge (04), $SiTa_2$ (11)
221	$\mathbb{Z}_4 \times \mathbb{Z}_8$	AlX (X = Sc, Y) (03) XB_6 (X = Ca, Sr, Ba) (03) BeTi (03), CaPd (20), $CsPbBr_3$ (23) $CsGeBr_3$ (23), $CsSnI_3$ (23) Ca_3PbO (22), XPt_3 (X = Pb, Sn) (34)

Table 2. TC insulating materials for $\mathcal{SG}$s191 and 194. These $\mathcal{SG}$s all own the same strong SI factor group, $\mathbb{Z}_{12}$, but with different other weak SI factor groups. The numbers in the parenthesis following the name of material are the nonvanishing SI in the corresponding X_{BS}. The SI is obtained by q_iC_i mod C_i, where $\mathbf{a}_i$ has a common factor larger than 1, which corresponds to the subscript of the factor groups of X_{BS}. The blue color denotes the materials carefully discussed in this work.

$\mathcal{SG}$	X_{BS}	Material (SI)
191	$\mathbb{Z}_6 \times \mathbb{Z}_{12}$	XB_2 (X = Mg, Ca) (52), SrB_2 (15), Ti (33)
194	$\mathbb{Z}_{12}$	AlLi (4), AlC_2Ta_3 (1), Ca_2NI (3) Graphite (4), Na_2CdSn (4) MgPo (1), $SiSr_2$ (1) Ti_2Sn (6)

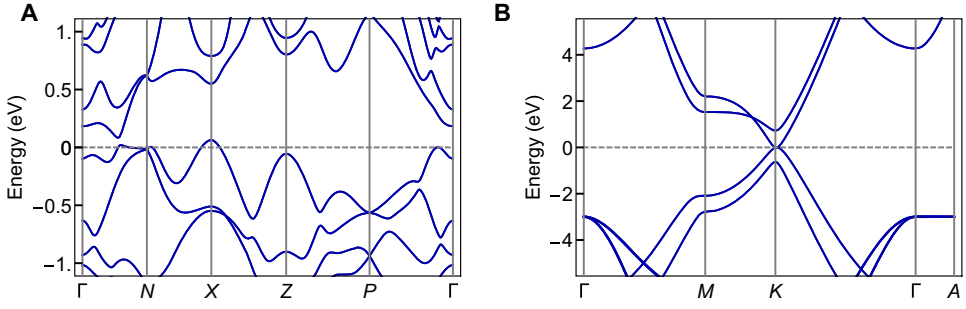

Fig. 1. Electronic band plots of TCIs. (**A**) Electronic band plot of TCI Pt_3Ge within $\mathcal{SG}$**140**. (**B**) Electronic band plot of TCI graphite within $\mathcal{SG}$**194**.

For Pt_3Ge, we find that the enriched inversion invariant κ_1 mod 4 (*31*, *32*) is also vanishing. Thus, this material has boundary states protected by symmetry operation containing n-fold axis ($n > 1$), mirror, and/or glide symmetries (*31*, *32*). Because of the rich point symmetry operations in $\mathcal{SG}$**140** (whose point group is D_{4h}), several topological phases may occur (*31*, *32*). We thus evaluate the mirror Chern numbers for the (001) (Miller indices with respect to the conventional lattice basis vectors) and (110) mirror planes by first-principles calculations. Our ab initio results show that they are also all vanishing. As shown in (*32*), with the above SI and mirror Chern numbers, the glide, screw, and S_4 invariants are thus nonvanishing (*31*, *32*): It would have glide-protected hourglass surface states in (100) glide symmetric planes as the corresponding invariant is 1. The C_{4z}-screw invariant is 1; thus, it would protect gapless hinge states along the **c** direction. We construct a tight binding (TB) model and fit its electronic structure, the SI, and all the topological invariants with the corresponding first-principles results. By the TB model, we demonstrate the surface hourglass band crossings as shown in the Supplementary Materials.

$\mathbb{Z}_{12}$ NONTRIVIAL TCI: GRAPHITE

We also searched the materials with $\mathcal{SG}$**194** ($P6_3/mmc$, whose point group is D_{6h}) in the database (*14*). We find that there are 52 and 254 materials belonging to cases 2 and 3, respectively. It is worth emphasizing that our results indicate that graphite (ICSD[14] 193439) is potentially a nontrivial insulator.

It is well known that graphene (i.e., monolayer of graphite) exhibits 2D massless Dirac excitation near K/K' points (*34*). The SO coupling (although small) opens a topological gap [~0.0008 meV (*35*)], making it, in principle, a 2D TI (*36*). The discovery of crystalline-symmetry–protected band topology in graphite, namely, the ABABABAB… Bernal stacking of graphene, demonstrates the possibilities of discovering various topological materials even among the simplest elemental materials. We thus present a detailed discussion in the following for graphite.

The $\mathcal{SG}$**194** owns nine AI basis vectors $\mathbf{a}_i^{\mathcal{SG}\mathbf{194}}$, $i = 1, 2, \ldots, 9$, where only the last one has a common factor, which is 12. Thus, $X_{\mathrm{BS}}^{\mathcal{SG}\mathbf{194}} = \mathbb{Z}_{12}$. The 16 valence bands in graphite are found to have the expansion coefficients $q = \left(2, 0, -1, -1, -1, -1, 1, 3, \frac{1}{3}\right)$ on the AI basis. Thus, the SI for graphite is $4 \in \mathbb{Z}_{12}$. The band structure is shown in Fig. 1B, where the SO coupling opens a small gap (around 0.025 meV) at the K point according to the first-principles calculation. The Fu-Kane strong and weak topological invariants (*15*) are found to be all vanishing as well as that κ_1 mod 4 is zero. We then calculate the (001) mirror Chern number at $k_z = 0$ by first-principles method and find that it is −2. Thus, there would be gapless Dirac surface states in the (001) mirror symmetric planes in the line $k_z = 0$. For another mirror symmetric plane, $k_z = \frac{\pi}{c}$ the mirror Chern number must be vanishing: for $\mathcal{SG}$**194**, $\mathcal{TJ}$ ($\mathcal{J}$ is the inversion) preserves the sign of the mirror eigenvalue, while it reverses the sign of Berry curvature: The Berry curvature for $+i$ mirror eigenvalue Ω_z^+ should satisfy $\mathcal{TJ}\Omega_z^+ = -\Omega_z^+ = 0$. We construct a TB model that reproduces the ab initio band structures very well and also gives the same SI and topological invariants to demonstrate the surface states protected by (001) mirror plane in the Supplementary Materials.

To ascertain graphite's nontrivial topology, we then calculate the $(\bar{1}20)$ plane's mirror Chern number and find that it is vanishing. Then, graphite would have sixfold screw-protected hinge states (*31*, *32*). It can also have glide- and rotation-protected surface states as dictated by the nonvanishing $C_2^{1\bar{1}0}$ (where the superscript of the point operation part denotes the rotation axis and the subscript denotes the rotation angle) rotation invariant and (010) glide invariant (*31*, *32*). While graphite is generally associated with small Fermi pockets, García *et al.* (*37*) proposed, based on the observation of a semiconducting gap in small samples of Bernal graphite, that these may arise from extrinsic effects. Thus, further experimental work would be of great interest.

THE OTHER DISCOVERED TCIS

Weak TI coexisting with TCI in $PbPt_3$ ($\mathcal{SG}$**221**) and Au_4Ti ($\mathcal{SG}$**87**)

The above two TC materials both have vanishing inversion and weak topological invariants. We also discover two materials, i.e., $PbPt_3$ (ICSD [14] 648399) in $\mathcal{SG}$**221** and Au_4Ti (ICSD[14] 109132) in $\mathcal{SG}$**87**, which have three weak topological indices (*15*) $\nu_i = 1$ for $i = 1, 2, 3$ (ν_0 is vanishing for both cases); however, they have different inversion topological invariants, i.e., κ_1 mod 4 (*31*, *32*) is equal to 0 or 2, respectively.

$PbPt_3$ crystallizes in the cubic structure with a primitive Bravais lattice. The electronic band structure is shown in Fig. 2A. The material has 34 valence electrons in the unit cell. The calculated $n_{\mathbf{k}}^{\alpha}$ for these 34 bands can be expanded on the 14 AI basis vectors of $\mathcal{SG}$**221**, and the expansion coefficients are $q = (0, 0, 0, 0, 0, -1, 1, 1, 0, 1, -1, -1, -\frac{1}{4}, -\frac{1}{2})$. The last two AI basis vectors own a common factor 4 and 8, respectively. Thus, the SI is $(3, 4) \in \mathbb{Z}_4 \times \mathbb{Z}_8$. On the other hand, the parity calculations show that it is a weak TI (*15*). To further pin down the precise topological character of the system, we also calculate the two mirror Chern numbers for (001) mirror plane ($k_z = 0$ or $\frac{\pi}{c}$) (*31*, *32*) and find that they are both equal to −1. This implies that the screw invariant of 2_1^{011}, as discussed in (*32*), is 1. Note that, as $\mathcal{SG}$**221** is symmorphic, the screw 2_1^{011} discussed above is not essential, in the sense that it is really a combination of the rotation C_2^{011} combined with a lattice translation with a nonzero parallel component along the 011 rotation axis. Nonetheless, on the appropriate surface termination, which, as a whole, respects this screw symmetry, one could find protected hinge states.

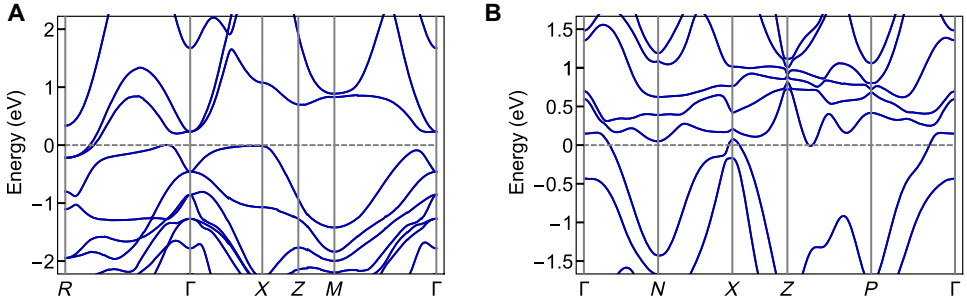

Fig. 2. Electronic band plots of TCIs. (**A**) Electronic band plot of $PbPt_3$ within $\mathcal{SG}$**221**. (**B**) Electronic band plot of Au_4Ti within $\mathcal{SG}$**87**.

Au_4Ti crystallizes in $\mathcal{SG}$**87** (*I*4/*m*), where Au and Ti occupy 8*h* and 2*a* Wyckoff positions, respectively. This material is found to belong to case 2. The electronic band structure is shown in Fig. 2B. We calculate the parities and find that its strong topological invariant (*15*) and inversion invariant κ_1 mod 4 (*31*, *32*) are both vanishing, while $\nu_1 = \nu_2 = \nu_3 = 1$, so it is a weak TI. Besides, the newly introduced invariant Δ (*31*) is found to be 4 (mod 8). Our first-principles calculations also show that the mirror Chern number for the (001) plane is vanishing. Thus, it would allow glide-protected hourglass surface states in glide $\{M_{001}|\frac{1}{2}\frac{1}{2}0\}$ symmetric plane (*31*, *32*). It can also host hinge states along the (001) direction, which are protected by the (nonessential) screws $\{C_2^{001}|00\frac{1}{2}\}$ or $\{C_4^{001}|00\frac{1}{2}\}$ (*32*).

TCI Ti_2Sn in $\mathcal{SG}$194

Ti_2Sn (ICSD[14] 182428) within $\mathcal{SG}$**194** is found to be a TCI. The electronic band structure plot is shown in Fig. 3. It has direct gaps everywhere, except in a small area where there are electron and hole pockets. Our calculations show that the SI is (6). Parity calculations show that the inversion invariant κ_1 mod 4 (*31*, *32*) is 2, while the strong and weak topological invariants (*15*) $\nu_{0,1,2,3}$ are all vanishing. From first-principles calculation, we find that the mirror Chern number for the $(\bar{1}20)$ plane is −4. This high mirror Chern number indicates that there should be multiple Dirac cones in the $(\bar{1}20)$ mirror symmetric plane. To identify the band topology, we also calculate the mirror Chern number of the (001) mirror plane, which is found to be vanishing. Thus, it can accommodate hourglass surface states in $\{M_{010}|00\frac{1}{2}\}$ or $\{M_{010}|\frac{1}{2}0\frac{1}{2}\}$ glide symmetric planes (*31*, *32*). C_2 around (010) can also protect surface Dirac cones (*31*, *32*). Besides, inversion and screw $\{C_6^{001}|00\frac{1}{2}\}$ can protect hinge states in corresponding hinges, satisfying the corresponding symmetries (*31*, *32*).

TOPOLOGICAL SEMIMETALS

Other than the TCIs, our method can also filter out topological (semi-) metals as by-products when the expansion coefficients belong to case 3. By further requiring relatively clean Fermi surfaces, we identify $AgXF_3$ (*X* = Rb, Cs; $\mathcal{SG}$**140**; ICSDs[14] 023153,023154) as good Dirac semimetals, with Dirac points pinned down to two HSPs (*P* and *N*) and AgAs*X* (*X* = Sr, Ba; $\mathcal{SG}$**194**; ICSDs[14] 049742,008278) as Dirac semimetals with symmetry-protected band crossing at the high-symmetry line, as shown in Fig. 4. These two materials families realize the two subcases within case 3 that we discussed. For the $AgXF_3$ family, the HSPs *P* and *N* both have only one 4D irrep, while the filling cannot be divided by 4. The filling-enforced Dirac points at *P* or *N* are subjected to more symmetry restrictions than those for the Dirac points in the high-symmetry line, and consequently, the Dirac dispersion is more isotropic. For the AgAs*X* family, in the high-symmetry line Γ-*A*, the Δ_7 and Δ_9 bands cross each other, resulting in a Dirac point protected by C_{6v}. It is worth pointing out that for AgAs*X*, the Fermi level exactly threads the Dirac point.

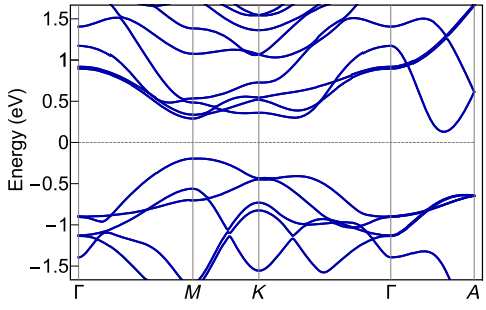

Fig. 3. Electronic band plot of TCI Ti_2Sn within $\mathcal{SG}$194.

CONCLUSIONS AND PERSPECTIVES

In this work, on the basis of our newly developed algorithm (*30*), we search for topological materials indicated by $\mathbb{Z}_8$ and $\mathbb{Z}_{12}$ strong factors in the SI groups. Focusing on $\mathcal{SG}$s **87**, **140**, **221**, **191**, and **194**, we predict many materials, which exhibit coexistence of various gapless boundary states due to the rich combination of various symmetry operators in these highly symmetric $\mathcal{SG}$*s*. Breaking the symmetry operation directly affects (move or even gap) the gapless topological boundary state; thus, one may easily tune the novel properties of these predicted topological materials through strain or boundary decoration.

It is worth mentioning that the electronic topological phenomenon is widespread in real materials, and as shown in fig. S3, most of the materials in the five $\mathcal{SG}$*s* we scanned belong to topological phases indicated by cases 2 and 3. Here, we only discuss the materials with clean Fermi surfaces, since in these materials we expect the transport properties to be dominated by the topologically nontrivial states. Our scheme also finds some good metals with big Fermi surfaces having nonzero SI. One good example is MgB_2. It is interesting to contemplate on the possible interplay between its superconductivity (*38*) and band topology.

We hope that our proposed materials will enrich the set of realistic topological crystalline materials and stimulate related experiments. With the demonstrated efficiency, our method (*30*) can be used for a large-scale systematic search of the entire materials database, which could lead to the discovery for many more new topological materials.

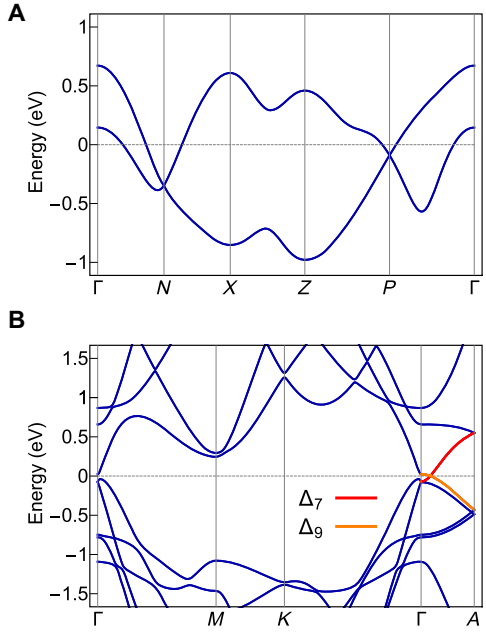

Fig. 4. Electronic band plots of Dirac semimetals. (**A**) $AgCsF_3$ within $\mathcal{SG}$**140** owns Dirac points pinned down at *P* and *N* points. (**B**) AgAsBa within $\mathcal{SG}$**194** has a Dirac point lying in the high-symmetry line Γ*A*. The Dirac point is protected by C_{6v}, and the band crossing arises from two twofold degenerate bands with different irreps (Δ_7 and Δ_9).

METHODS

The electronic band structure calculations were carried out using the full potential linearized augmented plane-wave method as implemented in the WIEN2k package (*39*). The generalized gradient approximation with Perdew-Burke-Ernzerhof (*40*) realization was adopted for the exchange-correlation functional.

SUPPLEMENTARY MATERIALS

Supplementary material for this article is available at http://advances.sciencemag.org/cgi/content/full/5/3/eaau8725/DC1

Section S1. First-principles calculated parities
Section S2. S_4 invariant materials
Section S3. Details of calculating mirror Chern numbers by first-principles method
Section S4. Details of the TB model and the glide/mirror-protected surface states
Section S5. AI basis vectors
Section S6. Materials statistics
Table S1. Ab initio calculated parities.
Table S2. Ab initio calculated κ_4 for body-centered lattice.
Table S3. Ab initio calculated κ_4 for primitive lattice.
Table S4. AI basis vectors in this work for $\mathcal{SG}$s **87**, **140**, and **221**.
Table S5. AI basis vectors in this work for $\mathcal{SG}$s **191** and **194**.
Fig. S1. TB fitting of Pt_3Ge and its surface states.
Fig. S2. TB fitting of graphite and its surface states.
Fig. S3. Materials statistics.
Source code

REFERENCES AND NOTES

1. M. Z. Hasan, C. L. Kane, Colloquium: Topological insulators. *Rev. Mod. Phys.* **82**, 3045 (2010).
2. X.-L. Qi, S.-C. Zhang, Topological insulators and superconductors. *Rev. Mod. Phys.* **83**, 1057 (2011).
3. C.-K. Chiu, J. C. Y. Teo, A. P. Schnyder, S. Ryu, Classification of topological quantum matter with symmetries. *Rev. Mod. Phys.* **88**, 035005 (2016).
4. L. Fu, Topological crystalline insulators. *Phys. Rev. Lett.* **106**, 106802 (2011).
5. R.-J. Slager, A. Mesaros, V. Juričić, J. Zaanen, The space group classification of topological band-insulators. *Nat. Phys.* **9**, 98–102 (2013).
6. Y. Ando, L. Fu, Topological crystalline insulators and topological superconductors: From concepts to materials. *Annu. Rev. Condens. Matter Phys.* **6**, 361–381 (2015).
7. T. H. Hsieh, H. Lin, J. Liu, W. Duan, A. Bansil, L. Fu, Topological crystalline insulators in the SnTe material class. *Nat. Commun.* **3**, 982 (2012).
8. W. A. Benalcazar, B. A. Bernevig, T. L. Hughes, Quantized electric multipole insulators. *Science* **357**, 61–66 (2017).
9. S. A. Parameswaran, Y. Wan, Viewpoint: Topological insulators turn a corner. *Physics* **10**, 132 (2017).
10. F. Schindler, A. M. Cook, M. G. Vergniory, Z. Wang, S. S. P. Parkin, B. A. Bernevig, T. Neupert, Higher-order topological insulators. *Sci. Adv.* **4**, eaat0346 (2018).
11. Z. Wang, A. Alexandradinata R. J. Cava, B. A. Bernevig, Hourglass fermions. *Nature* **532**, 189–194 (2016).
12. T. Bzdušek, Q. Wu, A. Rüegg, M. Sigrist, A. A. Soluyanov, Nodal-chain metals. *Nature* **538**, 75–78 (2016).
13. B. Bradlyn, J. Cano, Z. Wang, M. G. Vergniory, C. Felser, R. J. Cava, B. A. Bernevig, Beyond Dirac and Weyl fermions: Unconventional quasiparticles in conventional crystals. *Science* **353**, aaf5037 (2016).
14. M. Hellenbrandt, The Inorganic Crystal Structure Database (ICSD)—Present and future. *Crystallogr. Rev.* **10**, 17–22 (2004).
15. L. Fu, C. L. Kane, Topological insulators with inversion symmetry. *Phys. Rev. B* **76**, 045302 (2007).
16. C. Fang, L. Fu, Rotation anomaly and topological crystalline insulators. arXiv:1709.01929 (2017).
17. D. S. Freed, G. W. Moore, Twisted equivariant matter. *Ann. Henri Poincaré* **14**, 1927–2023 (2013).
18. K. Shiozaki, M. Sato, Topology of crystalline insulators and superconductors. *Phys. Rev. B* **90**, 165114 (2014).
19. K. Shiozaki, M. Sato, K. Gomi, Topology of nonsymmorphic crystalline insulators and superconductors. *Phys. Rev. B* **93**, 195413 (2016).
20. K. Shiozaki, M. Sato, K. Gomi, Topological crystalline materials: General formulation, module structure, and wallpaper groups. *Phys. Rev. B* **95**, 235425 (2017).
21. K. Shiozaki, M. Sato, K. Gomi, Atiyah-Hirzebruch spectral sequence in band topology: General formalism and topological invariants for 230 space groups. arXiv:1802.06694 [cond-mat.str-el] (19 February 2018).
22. C. Fang, M. J. Gilbert, B. A. Bernevig, Bulk topological invariants in noninteracting point group symmetric insulators. *Phys. Rev. B* **86**, 115112 (2012).
23. C. Fang, L. Fu, New classes of three-dimensional topological crystalline insulators: Nonsymmorphic and magnetic. *Phys. Rev. B* **91**, 161105(R) (2015).
24. X. Wan, A. M. Turner, A. Vishwanath, S. Y. Savrasov, Topological semimetal and Fermi-arc surface states in the electronic structure of pyrochlore iridates. *Phys. Rev. B* **83**, 205101 (2011).
25. H. Weng, C. Fang, Z. Fang, B. A. Bernevig, X. Dai, Weyl semimetal phase in noncentrosymmetric transition-metal monophosphides. *Phys. Rev. X* **5**, 011029 (2015).
26. S.-M. Huang, S.-Y. Xu, I. Belopolski, C.-C. Lee, G. Chang, B. Wang, N. Alidoust, G. Bian, M. Neupane, C. Zhang, S. Jia, A. Bansil, H. Lin, M. Z. Hasan, A Weyl Fermion semimetal with surface Fermi arcs in the transition metal monopnictide TaAs class. *Nat. Commun.* **6**, 7373 (2015).
27. H. C. Po, A. Vishwanath, H. Watanabe, Symmetry-based indicators of band topology in the 230 space groups. *Nat. Commun.* **8**, 50 (2017).
28. B. Bradlyn, L. Elcoro, J. Cano, M. G. Vergniory, Z. Wang, C. Felser, M. I. Aroyo, B. A. Bernevig, Topological quantum chemistry. *Nature* **547**, 298–305 (2017).
29. H. Watanabe, H. C. Po, A. Vishwanath, Structure and topology of band structures in the 1651 magnetic space groups. *Sci. Adv.* **4**, eaat8685 (2018).
30. F. Tang, H. C. Po, A. Vishwanath, X. Wan, Efficient topological materials discovery using symmetry indicators. arXiv:1805.07314 [cond-mat.mes-hall] (18 May 2018).
31. E. Khalaf, H. C. Po, A. Vishwanath, H. Watanabe, Symmetry indicators and anomalous surface states of topological crystalline insulators. *Phys. Rev. X* **8**, 031070 (2018).
32. Z. Song, T. Zhang, Z. Fang, C. Fang, Quantitative mappings between symmetry and topology in solids. *Nat. Commun.* **9**, 3530 (2018).
33. J. Kruthoff, J. de Boer, J. van Wezel, C. L. Kane, R.-J. Slager, Topological classification of crystalline insulators through band structure combinatorics. *Phys. Rev. X* **7**, 041069 (2017).
34. A. H. Castro Neto, F. Guinea, N. M. R. Peres, K. S. Novoselov, A. K. Geim, The electronic properties of graphene. *Rev. Mod. Phys.* **81**, 109 (2009).
35. Y. Yao, F. Ye, X.-L. Qi, S.-C. Zhang, Z. Fang, Spin-orbit gap of graphene: First-principles calculations. *Phys. Rev. B* **75**, 041401(R) (2007).
36. C. L. Kane, E. J. Mele, Quantum spin Hall effect in graphene. *Phys. Rev. Lett.* **95**, 226801 (2005).
37. N. García, P. Esquinazi, J. Barzola-Quiquia, S. Dusari, Evidence for semiconducting behavior with a narrow band gap of Bernal graphite. *New J. Phys.* **14**, 053015 (2012).
38. J. Nagamatsu, N. Nakagawa, T. Muranaka, Y. Zenitani, J. Akimitsu, Superconductivity at 39 K in magnesium diboride. *Nature* **410**, 63–64 (2001).
39. P. Blaha, K. Schwarz, G. Madsen, D. Kvasicka, J. Luitz, *WIEN2k: An Augmented Plane Wave Plus Local Orbitals Program for Calculating Crystal Properties* (Vienna University of Technology, 2001).
40. J. P. Perdew, K. Burke, M. Ernzerhof, Generalized gradient approximation made simple. *Phys. Rev. Lett.* **77**, 3865–3868 (1996).

Acknowledgments

Funding: F.T. and X.W. were supported by the National Key R&D Program of China (nos. 2018YFA0305704 and 2017YFA0303203), the NSFC (nos. 11525417, 11834006, 51721001, and 11790311), and the excellent programme in Nanjing University. F.T. was also supported by the program B for Outstanding PhD candidate of Nanjing University. X.W. was partially supported by a QuantEmX award funded by the Gordon and Betty Moore Foundation's EPIQS Initiative through ICAM-I2CAM, grant GBMF5305, and the Institute of Complex Adaptive Matter (ICAM). A.V. was supported by NSF DMR-1411343, a Simons Investigator grant, and the ARO MURI on TIs (grant W911NF- 12-1-0961). H.C.P. was supported by a Pappalardo Fellowship at MIT. **Author contributions:** X.W., A.V., and H.C.P. conceived and designed the project. F.T. performed ab initio calculations. All authors contributed to the writing and editing of the manuscript. **Competing interests:** The authors declare that they have no competing interests. **Data and materials availability:** All data needed to evaluate the conclusions in the paper are present in the paper and/or the Supplementary Materials. Our codes of symmetry-indicator method are present in https://datadryad.org/resource/doi:10.5061/dryad.8c3hr65. Additional data related to this paper may be requested from the authors.

Submitted 23 July 2018
Accepted 28 January 2019
Published 8 March 2019
10.1126/sciadv.aau8725

Citation: F. Tang, H. C. Po, A. Vishwanath, X. Wan, Topological materials discovery by large-order symmetry indicators. *Sci. Adv.* **5**, eaau8725 (2019).

Science Advances

Topological materials discovery by large-order symmetry indicators

Feng Tang, Hoi Chun Po, Ashvin Vishwanath and Xiangang Wan

Sci Adv **5** (3), eaau8725.
DOI: 10.1126/sciadv.aau8725